THE JOURNAL OF PHYSICAL CHEMISTRY A

Article

pubs.acs.org/JPCA

Vibrational Spectroscopy of Bisulfate/Sulfuric Acid/Water Clusters: Structure, Stability, and Infrared Multiple-Photon Dissociation Intensities

Tara I. Yacovitch,[†] Nadja Heine,[‡] Claudia Brieger,[‡] Torsten Wende,[‡] Christian Hock,[†] Daniel M. Neumark,*[,†,§] and Knut R. Asmis*[,‡]

[†]Department of Chemistry, University of California, Berkeley, California 94720, United States

[‡]Fritz-Haber-Institut der Max-Planck-Gesellschaft, Faradayweg 4-6, 14195 Berlin, Germany

[§]Chemical Sciences Division, Lawrence Berkeley National Laboratory, Berkeley, California 94720, United States

Supporting Information

ABSTRACT: The structure and stability of mass-selected bisulfate, sulfuric acid, and water cluster anions, $HSO_4^-(H_2SO_4)_m(H_2O)_n$, are studied by infrared photodissociation spectroscopy aided by electronic structure calculations. The triply hydrogen-bound $HSO_4^-(H_2SO_4)$ configuration appears as a recurring motif in the bare clusters, while incorporation of water disrupts this stable motif for clusters with $m > 1$. Infrared-active vibrations predominantly involving distortions of the hydrogen-bound network are notably missing from the infrared multiple-photon dissociation (IRMPD) spectra of these ions but are fully recovered by messenger-tagging the clusters with H_2. A simple model is used to explain the observed "IRMPD transparency".

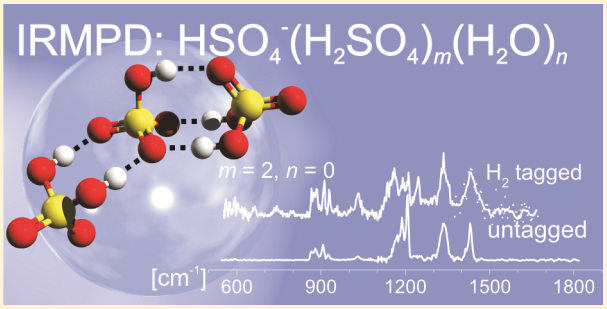

I. INTRODUCTION

Negatively charged clusters of sulfuric acid and water are abundant in the atmosphere, with $HSO_4^-(H_2SO_4)_m$, $m = 1-3$, accounting for 62% of the small stratospheric negative ions at 35 km.[1] Charged species are important in the early stages of atmospheric aerosol growth through the process of ion-induced nucleation,[2,3] with negative ions serving as more effective nucleation sites than positive ions.[4] Experimental aerosol growth studies for ionic clusters of sulfuric acid and water (charge carrier HSO_4^- or H^+) have been completed under a variety of conditions. These studies find that at room temperature, the uptake of sulfuric acid by negative ions is preferred to the uptake of water, as explained by the ability of H_2SO_4 to make stronger H-bonds to the negative HSO_4^- core.[5] At temperatures representative of the midtroposphere (248 K), ions of the type $HSO_4^-(H_2SO_4)_m(H_2O)_n$ are the dominant nucleating cluster. The presence of other species such as NH_3 is required to account for atmospheric observations in the warmer boundary layer (278–292 K).[6] In this paper, the structure and stability of $HSO_4^-(H_2SO_4)_m(H_2O)_n$ clusters are studied using infrared photodissociation (IRPD) spectroscopy in combination with electronic structure calculations. Moreover, infrared multiple-photon dissociation (IRMPD) spectra of $HSO_4^-(H_2SO_4)_m$ are compared to single-photon IRPD spectra of the corresponding H_2-tagged species in order to shed light on the nature of "IRMPD-transparent" vibrational modes.

In addition to the field studies that measure atomic masses and relative abundances of $HSO_4^-(H_2SO_4)_m(H_2O)_n$ species,[1,7−10] a number of kinetics studies have investigated small ionic clusters of strong acids.[11−14] These studies have yielded rate constants for the reaction of the clusters with sulfuric acid and other molecular acids like HNO_3. Enthalpies for the loss of a sulfuric acid molecule from $HSO_4^-(H_2SO_4)_m$ were found to hover around 100 kJ/mol for $m = 2-5$.[14] Gibbs free energies for several clustering reactions have been determined experimentally, showing stronger H_2SO_4 binding to anionic cores than to water. For example, the free energy change for clustering to a $HSO_4^-(H_2SO_4)_2$ core (at 233 K) is −26 kJ/mol for one water and −59 kJ/mol for a sulfuric acid molecule.[15]

The triply hydrogen-bound complex $HSO_4^-(H_2SO_4)$ has been studied theoretically by Evleth[16] and others.[17] The enthalpy of complexation was calculated to be −196 kJ/mol, higher than the values all other known hydrogen-bonded complexes. The barrier to transfer of a single proton, that is, $HSO_4^-(H_2SO_4) \rightarrow (H_2SO_4)HSO_4^-$, was found to be very low (8 kJ/mol), which suggests that the complex is approaching charge delocalization. This same structure along with several isomers of the $HSO_4^-(H_2SO_4)_2$ cluster has also been calculated by Hou et al.[18] As in other systems involving shared

Special Issue: Joel M. Bowman Festschrift

Received: January 5, 2013
Revised: May 7, 2013
Published: May 29, 2013

protons,[19−21] high anharmonicity is expected for shared proton vibrations.

IRPD spectroscopy is a powerful structural probe of these and other small atmospherically relevant clusters.[22] The hydrated bisulfate and sulfate systems $HSO_4^-(H_2O)_n$ and $SO_4^{2-}(H_2O)_n$ have been studied previously using this method.[23−25] The bisulfate system showed the formation of extensive H-bonding networks starting at $n = 3$, while spectra of the hydrated sulfate dianions indicated more ligand-like binding to the sulfate core, confirmed by recent high-level calculations up to $n = 6$.[26] Closure of the first hydration shell of the sulfate dianions at $n = 12$ was also inferred, though this conclusion has recently been questioned by Wan et al.[27] Finally, recent results on $HSO_4^-(H_2SO_4)_m(HNO_3)_n$ clusters show that strong hydrogen bonds allow variation in charge localization depending on composition.[28]

The dissociation limit of these clusters is considerably higher than the IR photon energy used to measure the photodissociation spectra, so absorption of multiple photons is required to detect photofragment ions. Hence, we refer to these spectra as IRMPD spectra. A complementary, often more difficult experiment involves adding a weakly bound messenger species such as He, Ne, Ar, or H_2 in order to bring the lowest dissociation limit of the complex below the photon energy.[29,30] To differentiate between the two experiments, we refer to the latter results as single-photon IRPD spectra even though, strictly speaking, we cannot exclude absorption of more than one photon during the vibrational predissociation process. The two types of experiments, with and without messenger-tagging, can lead to substantially different IR spectra, typically with certain IR-active modes missing from the IRMPD spectrum.[25,31,32] We find here that comparison of the IRMPD spectra to the corresponding single-photon IRPD spectra aids in identifying the mechanism for these missing peaks.

II. EXPERIMENTAL AND THEORETICAL METHODS

Experiments were carried out on a previously described ring electrode trap/time-of-flight (TOF) mass spectrometer[33,34] using the free electron laser for infrared experiments (FELIX).[35] Ions were produced by electrospray of a solution of 25 mM H_2SO_4 in a 1:4 water:acetonitrile mix. The negative ions were then transferred into a high-vacuum system. Parent ions were mass-selected in a quadrupole mass filter and focused into a ring electrode ion trap. To allow for continuous ion loading and ion thermalization, the trap was continuously filled with He gas at an ion trap temperature of 15 K. The trap gas was swapped with a 20% mix of H_2 in He for the tagged results. After the trap was filled for 99 ms, all ions were extracted from the ion trap, focused both temporally and spatially into the center of the extraction region of an orthogonally mounted linear TOF mass spectrometer, and irradiated with a single 10 μs FELIX macropulse ($\leq$50 mJ/pulse and ~0.25% RMS bandwidth). Under these conditions, most of the ions are thermalized at the trap temperature prior to IR irradiation.[36,37] IRPD and IRMPD spectra were recorded by monitoring all ion intensities simultaneously as the laser wavelength was scanned. The photodissociation cross section σ_{IRMPD} was determined from the relative abundances of the parent and photofragment ions, $I_p(\nu)$ and $I_f(\nu)$, respectively, and the frequency-dependent energy fluence (assuming a constant interaction area throughout the range of scanned wavelengths) $\varphi_e(\nu)$ using[38]

$$\sigma_{IRMPD} = -\ln[I_p(\nu)/(I_p + I_f)]/\varphi_e(\nu) \quad (1)$$

In the case of the H_2-tagged spectra, a single-photon process is assumed and intensities are normalized instead to the photon fluence,[39] $\varphi(\nu) = \varphi_e(\nu)/h\nu$, such that $\sigma \propto \sigma_{IRMPD}\nu$.

Electronic structure calculations were performed using the Gaussian 09 program.[40] Initial structures were constructed using a combination of chemical intuition and results from molecular dynamics conformational searching using MacroModel 9.9[41] and the OPLS_2005[42] force field. Optimized geometries and harmonic frequencies at the B3LYP/6-311+G(d,p) level of theory were used to determine preliminary energetic orderings. Final geometries and harmonic vibrational frequencies were calculated at the B3LYP/6-311++G(2df, 2pd) level. The MP2 method is often used to study weakly bound systems[43] because it accounts better for the dispersion needed to treat van der Waals forces. For comparison, MP2 calculations using the same basis set as well as a larger aug-cc-pV(T+d)Z basis were done for selected $m = 1$ or 2, $n = 0$−2 clusters (Supporting Information). Similar structures and energetic orderings were found, and while the MP2 frequencies were systematically higher than the corresponding B3LYP frequencies, they showed the same peak pattern with slightly different relative intensities. We use the B3LYP method because it yields reliable geometries, frequencies, and IR intensities at a reasonable computational cost, such that a consistent set of simulated spectra can be produced for the complete set of systems studied here.[22] Other methods yield more reliable relative energies and binding energies.[44] Structures are labeled in order of their relative energies, including zero-point energy (zpe) corrections. All B3LYP dissociation energies were counterpoise-corrected to account for basis set superposition error.[45]

III. RESULTS

Figure 1 shows IRPD spectra for the $HSO_4^-(H_2SO_4)_m(H_2O)_n(H_2)_z$ clusters. The results are spliced together from individual scans over various spectral regions. For each value of m, the hydrogen-tagged spectrum ($z \geq 1$) is shown, followed by the bare $HSO_4^-(H_2SO_4)_m$ cluster and, for $m < 3$, the spectra of hydrated clusters with $n = 1$ and $n = 2$. The value of z varied depending on trap conditions and cluster size, ranging from $z = 1$ (smaller clusters) to $z = 4$ (large clusters). The spectra can be divided into regions based on the types of vibrations present, consistent with experimental spectra and calculated frequencies from bulk studies of H_2SO_4 via thin film[46] and matrix isolation spectroscopy.[47] At low frequencies, ~550 cm^{-1}, OSO core bends of the HSO_4^- and H_2SO_4 molecules appear. Singly bound O−S stretches appear from 800 to 950 cm^{-1}. The double bonded S═O stretches fall in the 950−1500 cm^{-1} range, with the symmetric stretches, antisymmetric stretches, and combined S═O stretch/SOH bends roughly ordered in increasing energy. The higher-frequency portion of this range mostly consists of pure H_2SO_4 modes involving an antisymmetric O═S═O stretch and two SOH bends. Water bending modes of the hydrated clusters appear in the highest-energy region, 1600−1700 cm^{-1}. Two other classes of vibrations are expected in hydrogen-bound clusters such as these:[25] wagging of the SOH moieties and water librations. These types of vibrations can be mixed together and occur in the 650−800 cm^{-1} spectral range. This region is notably flat in all of the untagged experimental results.

dx.doi.org/10.1021/jp400154v | J. Phys. Chem. A 2013, 117, 7081−7090

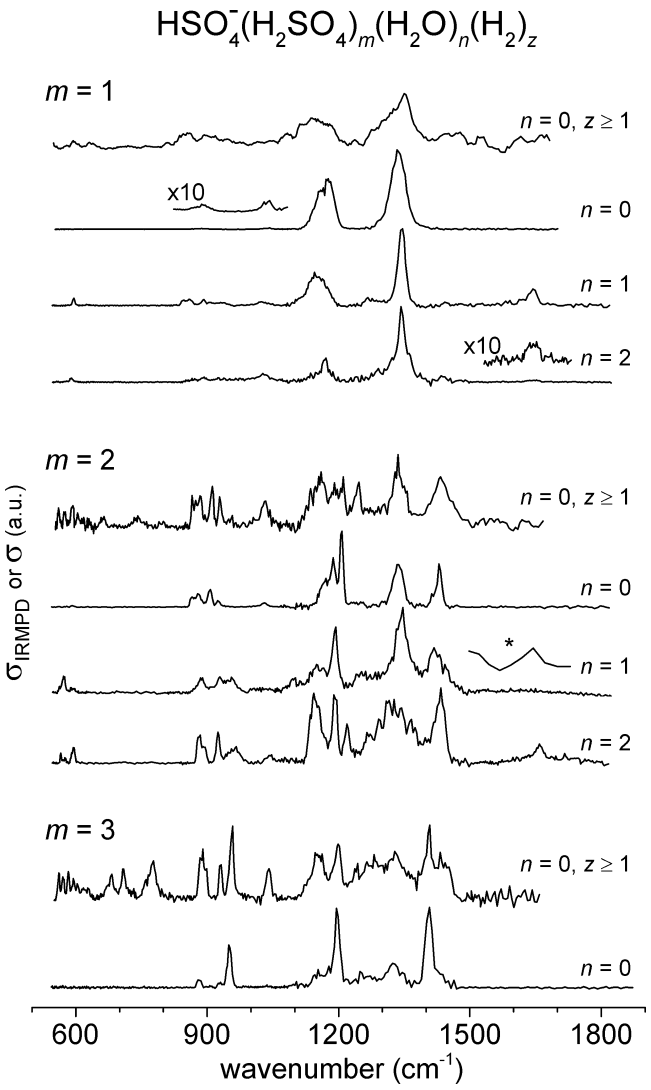

Figure 1. IRPD spectra for $HSO_4^-(H_2SO_4)_m(H_2O)_n(H_2)_z$ clusters. Each panel corresponds to a different number of H_2SO_4 ligands (m = 1−3). Hydrogen-tagged results ($z \geq 1$) for the bare $n = 0$ clusters are shown at the top of each m grouping. All other results are untagged ($z = 0$) and shown in order of increasing hydration (n = 0−2). The m = 1, $n = 0$, $z \geq 1$ spectrum was smoothed by weighted averaging of five neighboring points, as was the 1360−1680 cm^{-1} region of the $m = 2$, $n = 0$, $z \geq 1$ spectrum. The $m = 2$, $n = 1$ trace marked by an asterisk is part of an overview spectrum taken at higher laser power.

In comparing the untagged results in Figure 1, we observe a large increase in complexity upon addition of the second H_2SO_4 ($m = 1$ to $m = 2$) and less change upon the addition of the third. Hydration of the clusters makes little difference for $m = 1$ and more for $m = 2$. There are substantial differences between the hydrogen-tagged data and the IRMPD results from the corresponding untagged cluster. All features in the IRMPD results appear in the tagged results, but the reverse is not true. This IRMPD transparency is most noticeable in the water libration region, 600−800 cm^{-1}, where the $z \geq 1$ spectra show numerous additional peaks that are absent from the multiple-photon spectra.

IV. ANALYSIS AND DISCUSSION

The experimental results are compared to the simulated spectra computed at the B3LYP/6-311++G(2df, 2pd) level of theory in Figures 2−4. The lowest energy and best-fit simulated results are shown below the associated IRMPD spectra with many more spectra available in the Supporting Information. Calculated geometries are shown alongside the figures and are labeled numerically according to cluster size, with a "w" preceding the hydration number n. They are also labeled alphabetically in order of increasing relative energy, including zpe. For example, the **2w1c** isomer is the third-to-lowest energy structure found for the cluster with $m = 2$ and $n = 1$: $HSO_4^-(H_2SO_4)_2(H_2O)_1$. Stick spectra shown throughout correspond to the unscaled harmonic vibrational frequencies and doubly harmonic IR absorption intensities.

An additional goal of our analysis is to formulate a criterion for the IRMPD transparency mentioned in section III. With this in mind, individual frequency sticks in the simulated spectra are color-coded according to their normal mode character, with the goal of distinguishing between vibrations of the hydrogen-bound network and core vibrations like S═O stretching and OSO bending modes. As a first approximation, the percentage contributions of the hydrogen atoms to the normal mode displacements were computed. Using the mass-weighted displacements from the normal mode analysis, the Cartesian root mean squared (RMS) displacement for each atom (a) was calculated:

$$\mathrm{RMS_a} = \sqrt{\Delta x_a^2 + \Delta y_a^2 + \Delta z_a^2} \quad (2)$$

Then, the percentage contribution of the hydrogen atoms to the total displacements was calculated, $\%\mathrm{RMS_H} = (\mathrm{RMS_H}/\mathrm{RMS_{all}})\times 100\%$. In Figures 2−4, filtering of the modes is done according to the calculated $\%\mathrm{RMS_H}$ such that modes with a $\%\mathrm{RMS_H} > 75\%$ are shown in blue, while modes with a $\%\mathrm{RMS_H} \leq 75\%$ are shown in red.

Our hypothesis, considered in more detail in section IV.3, is that blue-colored features in the simulated spectra are more likely to be IRMPD-transparent, that is, seen in the tagged spectra only. The threshold value of 75% was chosen empirically such that the red stick spectrum gives a reasonable match to the untagged IRMPD results for the bare $n = 0$ clusters. In Figures 2−4, selected portions of each stick spectrum are convoluted with Gaussian peaks with 15 cm^{-1} fwhm for better comparability. For the $n = 0$ clusters, where tagging experiments are available for comparison, all peaks (blue and red) are included in the convolutions. For the $n \geq 1$ clusters, all peaks were convoluted (blue and red) for the higher-energy 1200−1900 cm^{-1} region, and only the low $\%\mathrm{RMS_H}$ peaks (red) are included in the convolutions for the 500−1200 cm^{-1} region. The high $\%\mathrm{RMS_H}$ vibrations are still shown in this region as blue sticks. The reasoning and implications behind this choice will be discussed below.

The hydrogen bond strengths mainly determine the cluster dissociation threshold and are important considerations in the interpretation of our spectra. To this end, the lowest dissociation energies for selected clusters are calculated and presented in Table 1. The trend in dissociation energies is as expected, scaling with number and strength of H-bonds, and spanning almost two orders of magnitude. Two isomers of the smallest cluster are compared, **1w0a** and **1w0b**, showing the nonadditive effects of two versus three hydrogen bonds. Subsequent entries show various loss pathways, always from a parent ion structure that includes the triply hydrogen-bound $HSO_4^-(H_2SO_4)$ structure: the loss of H_2SO_4, the loss of a single H_2O from the mono- or dihydrated triply H-bound

dx.doi.org/10.1021/jp400154v | J. Phys. Chem. A 2013, 117, 7081−7090

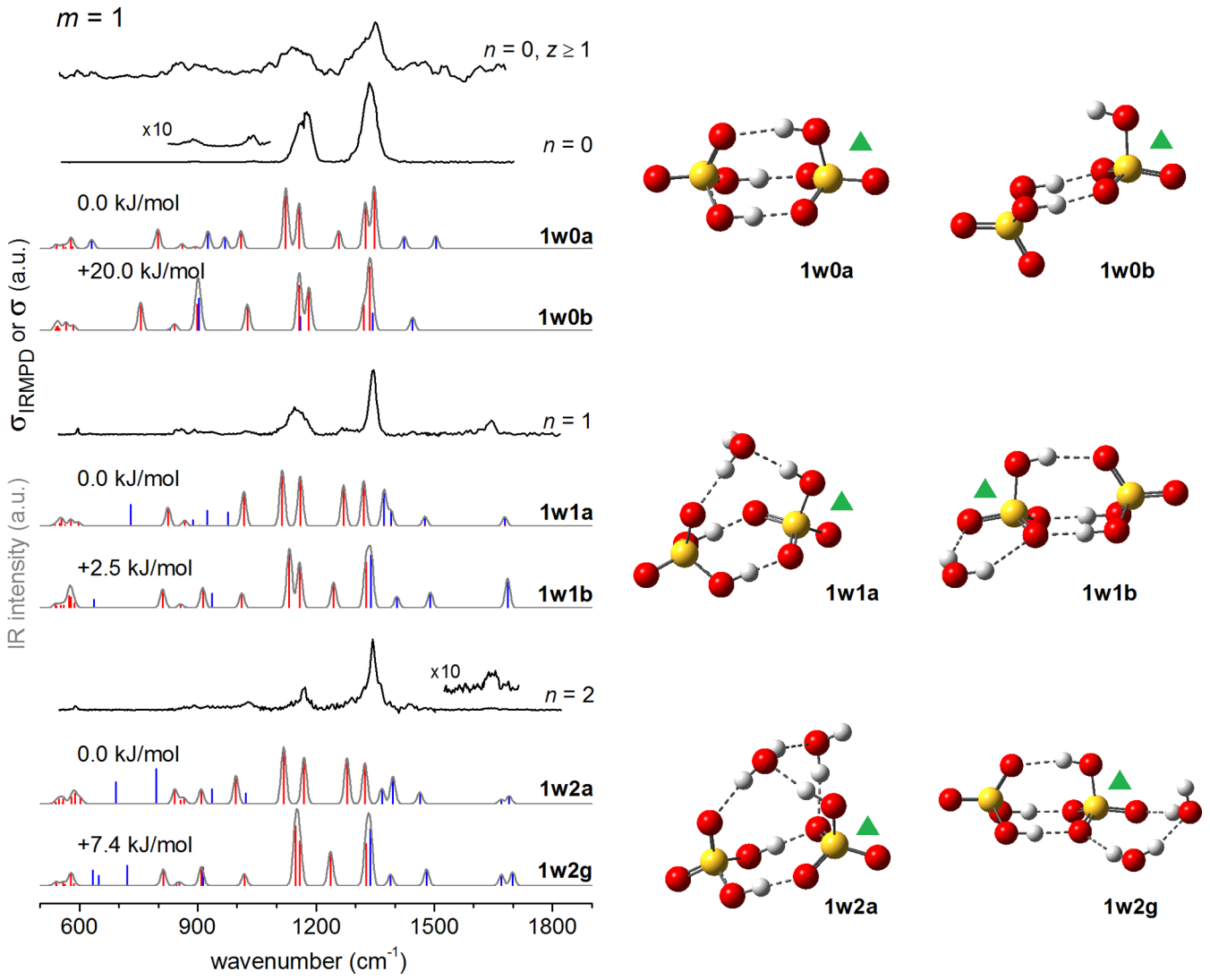

Figure 2. Comparison of experimental IRPD (black traces) and simulated linear absorption spectra (stick spectra) for the $HSO_4^-(H_2SO_4)_1(H_2O)_n$ clusters. Selected structures are shown on the right. The bisulfate moiety is indicated with a green triangle. The stick spectra are color-coded according to the degree of hydrogen motion for each mode, with $\%RMS_H < 75\%$ in red and $\%RMS_H \geq 75\%$ in blue. Gaussian convolutions of selected peaks of the stick spectra are shown in gray with a fwhm of 15 cm^{-1}.

cluster, and finally the loss of a H_2 tag molecule from a singly tagged **1w0a** cluster. On the basis of these values, the photodissociation at 1000 cm^{-1} of $HSO_4^-(H_2SO_4)$, $HSO_4^-(H_2SO_4)_2$, $HSO_4^-(H_2SO_4)(H_2O)$, and $HSO_4^-(H_2SO_4)(H_2)$ requires the energy of at least 12, 9, 3, and 1 photon(s), respectively. Thus, H_2-tagging indeed helps to probe the complexes in the linear absorption regime, whereas the IRMPD intensities of the bare bisulfate/sulfuric acid clusters may show pronounced nonlinear effects. Hydrated complexes lie in an intermediate regime.

1. Assignments. We first consider clusters with no water molecules ($n = 0$). For the smallest such cluster ($m = 1$, $n = 0$), the triply hydrogen-bound conformer **1w0a** (Figure 2) is calculated to be the lowest in energy with a predicted dissociation energy of 171 kJ/mol (Table 1), in agreement with previous results.[14,16,17] Rupture of the hydrogen bond donated by HSO_4^- leads to the second lowest energy conformer **1w0b** that lies 20.0 kJ/mol above the global minimum. Both structures yield similar IR spectra, but **1w0a** is in slightly better agreement with the H_2-tagged spectrum, both for the B3LYP and for the MP2 results (Supporting Information). While the intense core vibrations (red peaks in Figure 2) look similar for **1w0a** and **1w0b**, the less intense IR modes predicted for **1w0a** throughout the 550−1550 cm^{-1} region match the H_2-tagged spectrum better. The corresponding (untagged) IRMPD spectrum ($m = 1$, $n = 0$, $z = 0$) looks much simpler. Many of the weaker features observed in the H_2-tagged spectrum are missing. However, the untagged spectrum is largely consistent with the $\%RMS_H$-filtered results (red peaks only) of **1w0a**, with the only disagreement being the simulated peak at 1257 cm^{-1}. This peak, which appears weakly in the tagged spectrum, is in the S═O stretching region and is characteristic of the triply bound structure. It corresponds to the combined bisulfate SOH bend and S═O stretch and is discussed in more detail in section IV.3. Note the MP2 results (Supporting Information) suggest that B3LYP overestimates the IR intensity of this transition.

We next consider the $m = 2$, $n = 0$ cluster (Figure 3). Compared to that of the corresponding $m = 1$ cluster, the signal-to-noise in the tagged cluster spectrum improves

dx.doi.org/10.1021/jp400154v | J. Phys. Chem. A 2013, 117, 7081−7090

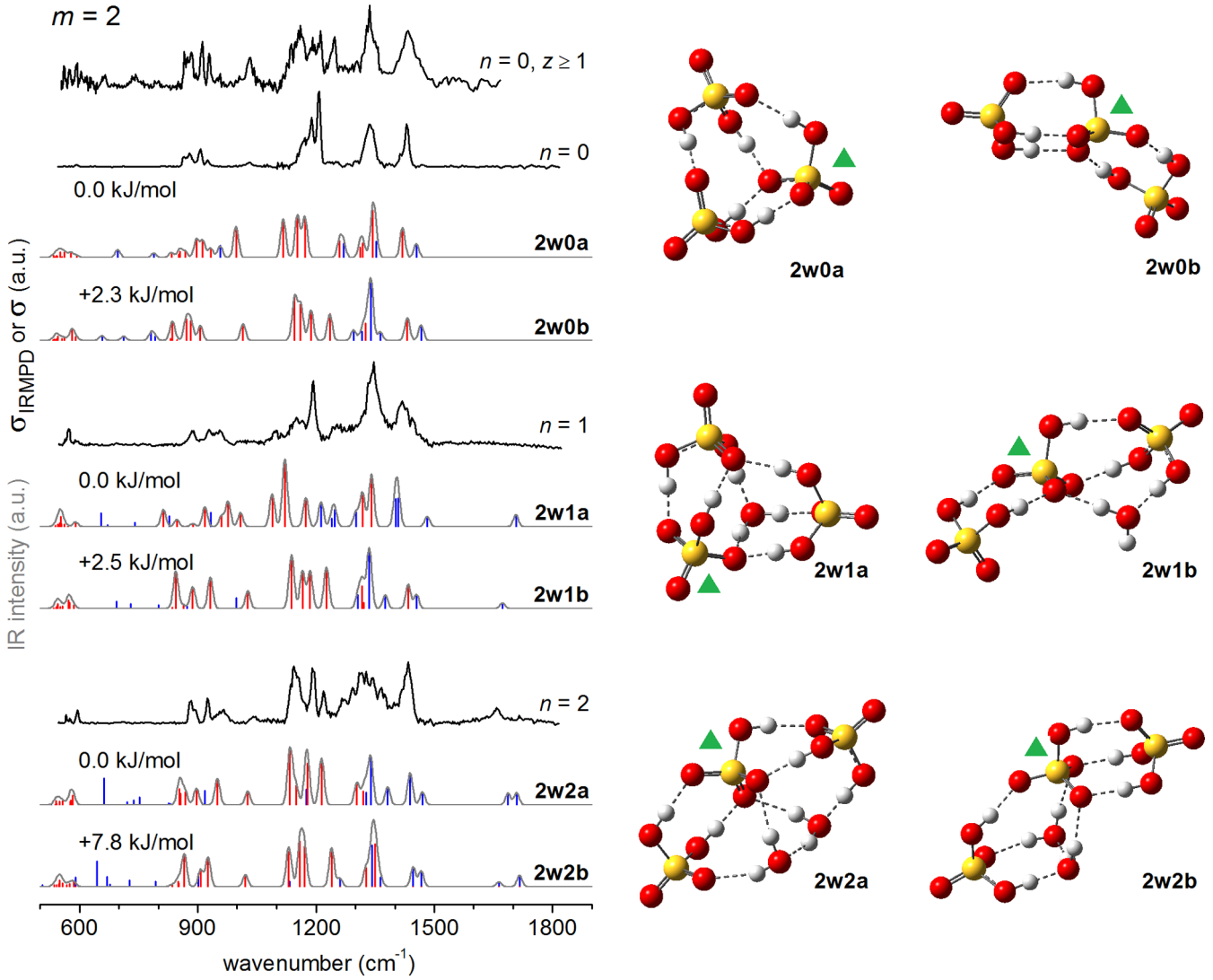

Figure 3. Comparison of experimental IRPD (black traces) and simulated linear absorption spectra (stick spectra) for the $HSO_4^-(H_2SO_4)_2(H_2O)_n$ clusters. Selected structures are shown on the right. The bisulfate moiety is indicated with a green triangle. The stick spectra are color-coded according to the degree of hydrogen motion for each mode, with $\%RMS_H < 75\%$ in red and $\%RMS_H \geq 75\%$ in blue. Gaussian convolutions of selected peaks of the stick spectra are shown in gray with a fwhm of 15 cm^{-1}.

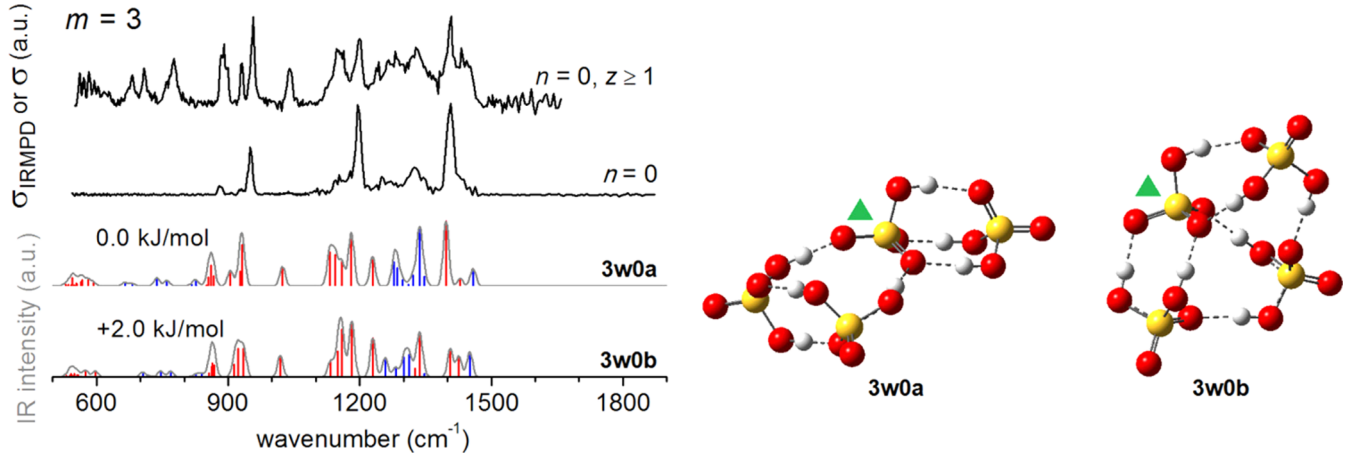

Figure 4. Comparison of experimental IRPD (black traces) and simulated linear absorption spectra (stick spectra) for the $HSO_4^-(H_2SO_4)_3$ cluster. Selected structures are shown on the right. The bisulfate moiety is indicated with a green triangle. The stick spectra are color-coded according to the degree of hydrogen motion for each mode, with $\%RMS_H < 75\%$ in red and $\%RMS_H \geq 75\%$ in blue. Gaussian convolutions of selected peaks of the stick spectra are shown in gray with a fwhm of 15 cm^{-1}.

dx.doi.org/10.1021/jp400154v | J. Phys. Chem. A 2013, 117, 7081−7090

Table 1. B3LYP/6-311++G(2df, 2pd) Dissociation Energies

formula	parent species	loss fragment	ionic fragment	dissociation energy[a] + zpe (kJ/mol)
$HSO_4^-H_2SO_4$	**1w0a**	H_2SO_4	HSO_4^-	171
$HSO_4^-H_2SO_4$	**1w0b**	H_2SO_4	HSO_4^-	153
$HSO_4^-(H_2SO_4)_2$	**2w0b**	H_2SO_4	**1w0a**	102
$HSO_4^-(H_2SO_4)(H_2O)$	**1w1b**	H_2O	**1w0a**	28
$HSO_4^-(H_2SO_4)(H_2O)_2$	**1w2l**[b]	H_2O	**1w1b**	24
$HSO_4^-(H_2SO_4)(H_2)$	**1w0a-H_2**[b]	H_2	**1w0a**	4[c]

[a]Dissociation energies are counterpoise corrected. [b]See Supporting Information for structures. [c]At this level of calculation (and at the MP2 level), inclusion of zpe results in a negative dissociation energy for the **1w0a-H_2** structure, so we show instead the electronic dissociation energy D_e = 4 kJ/mol. The experimentally estimated binding of a given H_2 molecule to a negatively charged cluster is around 7 kJ/mol (~600 cm^{-1}).[64]

substantially, allowing for easier comparison between single- and multiple-photon results. Full simulations (red and blue lines) of isomer **2w0b**, a bisulfate core between two H_2SO_4 molecules with the maximum possible five hydrogen bonds, capture most peak positions and intensities of the m = 2, n = 0, $z \geq 1$ experimental spectrum. This structure contains the triply hydrogen-bonded **1w0a** motif, with the second sulfuric acid binding via two donor hydrogen bonds to the bisulfate moiety. The structure **2w0a** recently reported by Hou et al.[18] involving a cyclic arrangement of the three cluster moieties is slightly lower in energy in our calculations as well, at the B3LYP and MP2 level of theories, but does not reproduce the spectrum quite as well as **2w0b**. Though agreement is still quite good, the cluster of peaks around 900 cm^{-1} is slightly broader than experiment, and the isolated peak at 994 cm^{-1} is too low in frequency. Structure **2w0d** (Supporting Information), in which the bisulfate anion occupies a terminal position, also does not reproduce the experimental data, especially in the ~1100−1200 cm^{-1} region. The **2w0c** structure (+0.4 kJ/mol, Supporting Information) differs only in the orientation of a H_2SO_4 molecule and gives a spectrum nearly identical to that of **2w0b**. The experimental IRMPD spectrum is missing several peaks seen in the tagged spectrum and, just as we noted for m = 1, agrees better with the red %RMS_H-filtered results. This spectrum also shows some intensity attenuation for the modes around 1150 cm^{-1} (concerted symmetric SO_2 stretches and S═O stretch/SOH bends of multiple moieties) that is discussed in section IV.3.

IR spectra of the largest bare cluster, $HSO_4^-(H_2SO_4)_3$, are shown in Figure 4. The lowest energy isomer **3w0a** matches the tagged experimental results well, particularly in the 1100−1500 cm^{-1} region. **3w0a** again contains the triply hydrogen-bound **1w0a** motif, with the two other sulfuric acid molecules hydrogen bound to each other while donating one hydrogen bond each to the bisulfate moiety. The next lowest isomer, **3w0b**, lies at 2.0 kJ/mol. Compared to **3w0a**, isomer **3w0b** does not show the same three distinct peaks in the S−OH stretching region around 900 cm^{-1}, all of which appear in the tagged spectrum. The first of these peaks (~860 cm^{-1}) is due to cluster-wide single-bonded S−OH stretches which appear in all isomers. The other two peaks, however, are due to antisymmetric S−OH stretches of H_2SO_4 in two distinct environments characteristic of **3w0a**: the terminal sulfuric acid in the **1w0a** motif (vibration at 905 cm^{-1}) and the two other H_2SO_4 molecules hydrogen bound to each other and to the bisulfate (two vibrations at ~930 cm^{-1}). The much higher-energy isomers **3w0e** and **3w0f** at 12 and 13 kJ/mol (Supporting Information) also contain the **1w0a** motif, but the remaining two H_2SO_4 molecules are in quite different hydrogen-bonding environments, spreading out the peaks in the S−OH stretching region.

The experimental IRMPD spectrum (z = 0) can be compared with the %RMS_H-filtered results (red lines only). Agreement with the **3w0a** simulations is good below 1200 cm^{-1}. Above 1200 cm^{-1}, agreement is also better with **3w0a** as long as all simulated lines (blue and red) are included. This is the same trend as will be observed for the water-solvated clusters. The simulated red line at 1023 cm^{-1}, a symmetric stretch of the HSO_4^- S═O bonds, is not observed in the untagged spectrum, which also shows intensity discrepancies for the first few peaks in the S═O stretching region around 1150 cm^{-1}.

Next we examine specific assignments of the IR bands in the spectra of the hydrated clusters that are also shown in Figures 2−4. A general comparison of the bare and hydrated clusters (Figure 1) shows very little change for m = 1 with increasing hydration, whereas m = 2 clusters display significant changes in the S═O stretching region, 1100−1500 cm^{-1}. This trend suggests that the m = 1 clusters retain the core structure upon hydration, while the hydrogen-bond network in the m = 2 cluster cores is disturbed by incorporation of water. Examination of the simulated geometries and structures shown on the right in Figures 2−4 sheds light on this hypothesis. In these simulations, only the %RMS_H-filtered results (red sticks) are included in the convolutions below 1200 cm^{-1}.

Two energetically low-lying isomers are found for the hydrated m = 1, n = 1 cluster. The B3LYP results (including zpe) predict **1w1b** 2.5 kJ/mol above **1w1a** (Figure 2), while the order is reversed in the MP2 results (Supporting Information), with **1w1b** 0.8 kJ/mol below **1w1a**. Best agreement is found with **1w1b** (2.5 kJ/mol), which has a triply hydrogen-bound structure with water binding loosely to the outside. Agreement is also comparable with the **1w1c** isomer (Supporting Information), another structure with the triply hydrogen-bound motif. The **1w1a** structure, with a water breaking apart the **1w0a** motif, has too many peaks in the 1100−1500 cm^{-1} region. Analogously, the m = 1, n = 2 cluster seems to agree best with the higher-energy isomer **1w2g** at 7.4 kJ/mol (MP2: 7.2 kJ/mol), showing the triply hydrogen-bound motif, based on the two intense, narrow peaks at 1150 and 1350 cm^{-1}. The lower energy isomers have structures where one or both water molecules are between the HSO_4^- and H_2SO_4, but these isomers show two doublets in the S═O stretching region. The high relative energy of the best-fit isomer puts this assignment in question, and without tagged results for m = 1, n = 2, the true structure of m = 1, n = 2 remains uncertain.

Both water-solvated clusters for m = 2 are assigned to their calculated lowest energy isomers. These minimum energy isomers are structures where water molecules donate or accept hydrogen bonds from all three core molecules and are well-incorporated into the cluster. Isomers where the triply hydrogen-bound motif persists (**2w1c** and **2w2b**, Figure 3 and Supporting Information) have too few peaks in the 1100−1250 cm^{-1} region. The addition of a second H_2SO_4 ligand thus allows incorporation of water molecules that disrupt the triply hydrogen-bound $HSO_4^-(H_2SO_4)$ motif. This second H_2SO_4

dx.doi.org/10.1021/jp400154v | J. Phys. Chem. A 2013, 117, 7081−7090

binds at the bisulfate, drawing away negative charge and weakening the $HSO_4^-(H_2SO_4)$ H-bonds.

In all of the hydrated clusters, water seems to be acting like a tag in the sense that the high $\%RMS_H$ peaks above 1200 cm^{-1} are observed (e.g., the peaks at ~1400 cm^{-1}) and their intensities are qualitatively comparable to the simulated results. This inference is in agreement with (a) the calculated binding energy of water to bisulfate, which is less than one-third that of sulfuric acid to bisulfate (Table 1), and (b) the observed fragmentation pattern of the larger clusters, in which significant water loss occurs with only small contributions of the total fragment ion signal coming from acid loss. The main intensity discrepancies are for the modes at ~1150 cm^{-1}. This discrepancy persists for $n = 1$ but disappears for the largest clusters with $n = 2$. This trend suggests that the more water molecules that are present, the more effective they are at recovering the linear IR intensities, even for structures where they make several hydrogen bonds. The main exception to this "water as a tag" mechanism is found at the lowest excitation energies probed, the region from 600 to 800 cm^{-1}, where the high $\%RMS_H$ peaks (blue sticks) are absent for $HSO_4^-(H_2SO_4)_m(H_2O)_n$, $m = 1$ or 2, $n = 1$ or 2.

2. Comparison with Bulk Results. Extensive experimental work has been done on concentrated sulfuric acid.[46,48,49] Figure 5 compares condensed phase IR spectra to those of the tagged

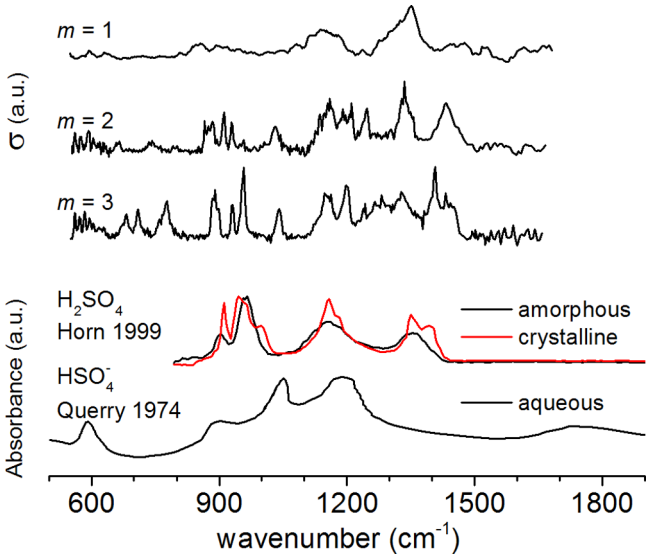

Figure 5. Comparison of the IRPD spectra of $HSO_4^-(H_2SO_4)_m(H_2)_z$ clusters to IR spectra of condensed phase samples from Horn et al.[46] showing H_2SO_4 peaks and Querry et al.[50] showing HSO_4^- peaks.

clusters ($n = 0$). The bulk results include pure H_2SO_4 amorphous and crystalline thin film spectra measured by Horn et al.[46] and spectra of aqueous HSO_4^- containing no molecular H_2SO_4 from Querry et al.[50] The thin film results show three clusters of peaks around 900−1150, 1100−1200, and 1350−1450 cm^{-1}, which sharpen upon cooling to 190 K (amorphous film → crystalline film). These results are from films of molecular H_2SO_4 formed in high-vacuum chambers by evaporation of trace H_2O. Lower resolution IR dilution studies by Walrafen et al.[48] (not shown) show broadened structure in similar regions and note that the peak around 1370 cm^{-1} in the spectrum of 99% composition sulfuric acid solutions disappears upon dilution to 80% sulfuric acid, where only bisulfate but no molecular H_2SO_4 remains. In fact, this diluted spectrum resembles the pure bisulfate spectrum reported by Querry et al. shown at the bottom of Figure 5.

These bulk spectra can be examined in light of the assigned cluster geometries and calculated normal modes of $HSO_4^-(H_2SO_4)_m$. The $m = 1$ cluster matches neither individual spectra for bulk H_2SO_4 or HSO_4^- nor a sum of the two. The $m = 2$ and $m = 3$ cluster results, on the other hand, exhibit intense peaks around 1200 and 1400 cm^{-1} with a peak spacing similar to the amorphous and crystalline thin film H_2SO_4 results, though slightly blue-shifted. The $m = 2$ and $m = 3$ clusters will have H_2SO_4 geometries that are less perturbed than that of the smaller $m = 1$ cluster, and their spectra will therefore be more similar to those of H_2SO_4 in thin films. The main difference is the region around 1300 cm^{-1}, which shows a clear peak in the cluster results that is missing in the H_2SO_4 amorphous and crystalline films. In the triply hydrogen-bound structures **1w0a**, **2w0b**, and **3w0a**, this ~1300 cm^{-1} peak corresponds to the combined SOH bend and S═O stretch vibrations of the bisulfate and the sulfuric acid involved in the triply hydrogen-bound motif. Thus, if this bisulfate mode is ignored, these small clusters ($m = 2$ or 3) show spectra strikingly similar to the bulk results, suggesting that additional cluster size-dependent changes in sulfuric acid modes will be small.

3. IRMPD Transparency Mechanism. The results shown in Figures 2−4 allow us to directly compare the spectra of cold clusters that dissociate via a single-photon process (tagged spectra, $z \geq 1$) to those of the analogous cluster dissociating via a multiple-photon process. IRMPD-transparent features are defined as the peaks that appear solely in the tagged results and are concentrated mostly in the water libration and SOH wagging region, as already noted in previous work.[25] The predicted IRMPD-transparent modes correspond to blue-colored sticks in the linear IR simulations; these vibrations have a high degree of H atom motion and a $\%RMS_H \geq 75\%$. In the following section, we discuss the mechanisms by which IRMPD spectra can differ from the messenger-tagged experiments ($z \geq 1$) and how well the $\%RMS_H$ measure succeeds in identifying those simulated peaks which are most likely to be IRMPD-transparent.

The IRPMD mechanism that is assumed to be occurring in our experiments is the incoherent multiple-photon absorption mechanism described in refs 51 and 52. It involves two key ingredients: fast energy dissipation in the form of intramolecular vibrational relaxation (IVR) and semiresonant absorption zones. The first photon is resonantly absorbed in a given mode. Because of anharmonic coupling, this energy is quickly (with respect to the macropulse length) redistributed over the bath of vibrational background states, effectively de-exciting this mode and allowing subsequent photons to be resonantly absorbed by the same transition. As the internal energy increases through multiple absorption and IVR cycles, the density of states reaches a point at which the IVR lifetime broadening of the zero-order vibrational levels approaches or even exceeds the average mode spacing, the so-called quasi-continuum.[53,54] In this region, semiresonant absorption occurs in zones near the original fundamental transition, eventually leading to dissociation.[52] This mechanism has two main requirements, either of which may disrupt it and result in differences between the multiple-photon experiment and the single-photon experiment (or linear IR simulation): (i) IVR must be efficient for all modes from the start, and (ii) the

dx.doi.org/10.1021/jp400154v | J. Phys. Chem. A 2013, 117, 7081−7090

fundamental frequency of the absorber must not change significantly early in the process, for example, through a geometry change. Condition (ii) is similar to the requirement of similar cross sections for each subsequent absorption,[55] an indication that the normal mode, and its dipole moment change, must be conserved.

A mechanism involving (i) has been explored in the OH stretch region by Pankewitz et al.[32] for the $NH_4^+(H_2O)$ cation and used to analyze a slew of previous experimental results on singly hydrated cationic systems. When the cluster dissociation energy is high, the IRMPD spectra show unexpectedly low peak intensities for the antisymmetric water OH stretch compared to those for the symmetric stretch. This effect is less pronounced or disappeared entirely upon addition of more water ligands or tags such as Ar, H_2, and N_2 and was postulated to originate from lowered relative coupling of the antisymmetric stretch to a vibration which weakens the dissociating H-bond. Beck and Lisy[31] also assume uncoupled oscillators to explain the IRMPD spectra of hydrated alkali metal cations.

A likelier mechanism here involves (ii), whereby certain resonant frequencies dramatically change during the early stages of the IRMPD absorption process. This selective IRMPD transparency has been postulated to originate from the disruption of the hydrogen-bond network.[31,56] For example, the first photon can excite a vibration, breaking one of the multiple hydrogen bonds without dissociating the cluster. This may be enough to change the frequency of the vibration and put it out-of-resonance with the light, at which point absorption is quenched and no dissociation occurs. The $\%RMS_H$-filtering method is a fast and simple way, especially for these large clusters, of identifying those modes which involve the hydrogen-bond network and are therefore most likely to be IRMPD-transparent. Low frequency modes are particularly prone to IRMPD transparency because they typically require several absorption events before reaching the quasi-resonant absorption region, whereas higher frequency modes require fewer or only one. This effect is seen experimentally: the high $\%RMS_H$ modes above ~1200 cm^{-1} are not IRMPD-transparent, except perhaps in the smaller, more tightly bound bare ($n = 0$) clusters with $m = 1$ or 2 (Figures 2 and 3), where both the dissociation energy and the transition to the quasi-continuum are higher. IRMPD transparency can be reduced by lowering the dissociation limit. Indeed, the tagged experimental spectra show excellent agreement with all simulated peaks, both red and blue.

Some vibrations with intermediate $\%RMS_H$ values present a challenge for this simple filtering method, such as the seemingly extra peaks noted earlier in the simulated $m = 1$, $n = 0$ spectra that are absent in the experimental IRMPD spectrum. The **1w0a** peak at 1257 cm^{-1} has a $\%RMS_H = 63\%$, and the **1w0b** peak at 898 cm^{-1} has a $\%RMS_H = 56\%$, putting these modes at a higher level of H-atom displacement than the majority of visible modes but also at a lower level than some of the strong IRMPD-visible features at 1300 cm^{-1}. We postulate that some aspect of the ability of these normal modes to disrupt the H-bond network is not fully captured by the $\%RMS_H$ measure. For example, the 1257 cm^{-1} mode contains a large amplitude SOH bend which breaks one of the three H-bonds, while the 898 cm^{-1} peak also involves some SOH wagging. Localization of the normal modes may also be an issue. In $m = 3$, $n = 0$, $z = 0$, the peaks at ~1150 cm^{-1} show up with lower than expected intensity. These modes are combinations of SOH bends and S═O stretches occurring on multiple moieties with $\%RMS_H$ on the order of 20−30%, while the neighboring transitions are similar, but localized to a single moiety.

Ultimately, dynamical methods[57−61] may be useful in teasing out the remaining details of the IRMPD-transparent modes in highly hydrogen-bound clusters. Such calculations would be able to trace the cluster frequencies as a function of temperature (i.e., as a function of number of photons absorbed) and would even be able to probe the redistribution of energy to the molecule when a given bond is excited.[62] The frequency information that is obtained from these calculations bypasses the normal mode treatment and may be advantageous in cases of large-amplitude motions, such as for the protons in the **1w0a** structure.[16] Finally, the IRMPD transparency model involves changes to individual frequencies as the H-bond network is perturbed. The effect of geometry changes on frequencies has recently been computed by multimode/vibrational configuration interaction for the $H_5O_2^+$ dimer, which showed that the low frequency intermolecular modes are most affected.[63] The $H_5O_2^+$ study involved scanning the torsional coordinate, but such a method could easily be extended to a single H-bond breaking coordinate (e.g., libration of a single H_2O) in our hydrogen-bound clusters.

V. CONCLUSIONS

From the tagged and untagged spectra of these clusters of bisulfate, sulfuric acid, and water, we can draw several conclusions. All pure clusters (i.e., no water) studied here exhibit a triple hydrogen bond between the bisulfate and one of the sulfuric acid molecules. Addition of water molecules has different effects depending on the size of the anion core. For the smallest cluster studied, $HSO_4^-(H_2SO_4)$, the triply hydrogen-bound motif appears to be retained upon hydration up to $n = 2$, while the larger $HSO_4^-(H_2SO_4)_2$ cluster shows incorporation of water molecules between the acid moieties and breaking of the triply hydrogen-bound motif.

Several of the clusters studied here and previously[25] show a large degree of IRMPD transparency associated with normal modes that are localized on the hydrogen-bonding network. The calculated $\%RMS_H$ gives a first-order quantitative measure of this H-bond flexion. Tagging these clusters with H_2 effectively recovers these IRMPD-transparent peaks. The intensities of all peaks, including those appearing in both tagged and untagged results, are closer to their calculated linear values upon tagging. These highly hydrogen-bound clusters would be ideal candidates for dynamics simulations in order to explore the frequencies, time scales, and trajectories involved in multiple-photon-induced dissociation.[62]

In the hydrated clusters, peaks that are predicted to be IRMPD-transparent based on the amount of hydrogen atom motion in the normal mode are observed, and peak intensities are closer to their simulated values with increasing hydration. The major exception to this trend is in the water libration region around 600−800 cm^{-1} where no peaks are observed in the IRMPD spectra, exactly as was the case for the previous $HSO_4^-(H_2O)_n$ and $HCO_3^-(H_2O)_n$ results. This indicates that the IRMPD experiments on water-solvated clusters are closer to single-photon results than those on bare structures, but also that there is no substitute for true tagging experiments with more weakly bound species in order to recover single-photon spectra.

■ ASSOCIATED CONTENT

Supporting Information

Comparisons of experimental IRMPD and additional simulated linear absorption spectra for the $HSO_4^-(H_2SO_4)_m(H_2O)_n$ clusters, structures used in the calculation of Table 1 dissociation energies, tabulated energetics, and comparisons with the MP2 method. This material is available free of charge via the Internet at http://pubs.acs.org.

■ AUTHOR INFORMATION

Corresponding Author

*D.M.N.: Department of Chemistry, University of California, Berkeley, CA 94720; E-mail, dneumark@berkeley.edu; Tel, 510-643-3502. K.R.A: Fritz-Haber-Institut der Max-Planck-Gesellschaft, Faradayweg 4-6, 14195 Berlin, Germany; E-mail, asmis@fhi-berlin.mpg.de; Tel, +49 30 8413 5735.

Notes

The authors declare no competing financial interest.

■ ACKNOWLEDGMENTS

We thank the Stichting voor Fundamenteel Onderzoek der Materie (FOM) for granting the required beam time and greatly appreciate the skill and assistance of the FELIX staff. This research is funded by the European Community's Seventh Framework Program (FP7/2007-2013, Grant 226716) and the Air Force Office of Scientific Research (FA9550-12-1-1060). T.I.Y. thanks the National Science and Engineering Research Council of Canada (NSERC) for a postgraduate scholarship. C.H. thanks the German Academic Exchange Service (DAAD) for a postdoctoral scholarship. Most calculations were performed at the Molecular Dynamics and Computational Facility at the University of California, Berkeley (National Science Foundation Grant CHE-0840505).

■ REFERENCES

(1) Arijs, E.; Nevejans, D.; Frederick, P.; Ingels, J. Negative-Ion Composition Measurements in the Stratosphere. *Geophys. Res. Lett.* **1981**, *8*, 121−124.

(2) Arnold, F. Atmospheric Ions and Aerosol Formation. *Space Sci. Rev.* **2008**, *137*, 225−239.

(3) Hirsikko, A.; Nieminen, T.; Gagne, S.; Lehtipalo, K.; Manninen, H. E.; Ehn, M.; Horrak, U.; Kerminen, V. M.; Laakso, L.; McMurry, P. H.; et al. Atmospheric Ions and Nucleation: A Review of Observations. *Atmos. Chem. Phys.* **2011**, *11*, 767−798.

(4) Enghoff, M. B.; Svensmark, H. The Role of Atmospheric Ions in Aerosol Nucleation−A Review. *Atmos. Chem. Phys.* **2008**, *8*, 4911−4923.

(5) Wilhelm, S.; Eichkorn, S.; Wiedner, D.; Pirjola, L.; Arnold, F. Ion-Induced Aerosol Formation: New Insights from Laboratory Measurements of Mixed Cluster Ions $HSO_4^-(H_2SO_4)_a(H_2O)_w$ and $H^+(H_2SO_4)_a(H_2O)_w$. *Atmos. Environ.* **2004**, *38*, 1735−1744.

(6) Kirkby, J.; Curtius, J.; Almeida, J.; Dunne, E.; Duplissy, J.; Ehrhart, S.; Franchin, A.; Gagne, S.; Ickes, L.; Kurten, A.; et al. Role of Sulphuric Acid, Ammonia and Galactic Cosmic Rays in Atmospheric Aerosol Nucleation. *Nature* **2011**, *476*, 429−433.

(7) Arnold, F.; Bohringer, H.; Henschen, G. Composition Measurements of Stratospheric Positive-Ions. *Geophys. Res. Lett.* **1978**, *5*, 653−656.

(8) Arnold, F.; Henschen, G. 1st Mass Analysis of Stratospheric Negative-Ions. *Nature* **1978**, *275*, 521−522.

(9) Arnold, F.; Fabian, R.; Ferguson, E. E.; Joos, W. Mass Spectrometric Measurements of Fractional Ion Abundances in the Stratosphere—Negative Ions. *Planet. Space Sci.* **1981**, *29*, 195−203.

(10) Arijs, E.; Nevejans, D.; Ingels, J.; Frederick, P. Negative-Ion Composition and Sulfuric-Acid Vapor in the Upper-Stratosphere. *Planet. Space Sci.* **1983**, *31*, 1459−1464.

(11) Viggiano, A. A.; Perry, R. A.; Albritton, D. L.; Ferguson, E. E.; Fehsenfeld, F. C. The Role of H_2SO_4 in Stratospheric Negative-Ion Chemistry. *J. Geophys. Res., C: Oceans Atmos.* **1980**, *85*, 4551−4555.

(12) Viggiano, A. A.; Henchman, M. J.; Dale, F.; Deakyne, C. A.; Paulson, J. F. Gas-Phase Reactions of Weak Brønsted Bases I^-, PO_3^-, HSO_4^-, FSO_3^-, and $CF_3SO_3^-$ with Strong Brønsted Acids H_2SO_4, FSO_3H, and CF_3SO_3H. A Quantitative Intrinsic Superacidity Scale for the Sulfonic Acids XSO_3H (X = HO, F, and CF_3). *J. Am. Chem. Soc.* **1992**, *114*, 4299−4306.

(13) Viggiano, A. A.; Seeley, J. V.; Mundis, P. L.; Williamson, J. S.; Morris, R. A. Rate Constants for the Reactions of $XO_3^-(H_2O)_n$ (X = C, HC, and N) and $NO_3^-(HNO_3)_n$ with H_2SO_4: Implications for Atmospheric Detection of H_2SO_4. *J. Phys. Chem. A* **1997**, *101*, 8275−8278.

(14) Lovejoy, E. R.; Curtius, J. Cluster Ion Thermal Decomposition (II): Master Equation Modeling in the Low-Pressure Limit and Fall-Off Regions. Bond Energies for $HSO_4^-(H_2SO_4)_x(HNO_3)_y$. *J. Phys. Chem. A* **2001**, *105*, 10874−10883.

(15) Viggiano, A. A.; Perry, R. A.; Albritton, D. L.; Ferguson, E. E.; Fehsenfeld, F. C. Stratospheric Negative-Ion Reaction-Rates with H_2SO_4. *J. Geophys. Res., C: Oceans Atmos.* **1982**, *87*, 7340−7342.

(16) Evleth, E. M. Theoretical Characterization of the Triply H-Bonded Complex Formed from HSO_4^- and H_2SO_4. *J. Mol. Struct.: THEOCHEM* **1994**, *307*, 179−185.

(17) Curtius, J.; Froyd, K. D.; Lovejoy, E. R. Cluster Ion Thermal Decomposition (I): Experimental Kinetics Study and Ab Initio Calculations for $HSO_4^-(H_2SO_4)_x(HNO_3)_y$. *J. Phys. Chem. A* **2001**, *105*, 10867−10873.

(18) Hou, G.-L.; Lin, W.; Deng, S. H. M.; Zhang, J.; Zheng, W.-J.; Paesani, F.; Wang, X.-B. Negative Ion Photoelectron Spectroscopy Reveals Thermodynamic Advantage of Organic Acids in Facilitating Formation of Bisulfate Ion Clusters: Atmospheric Implications. *J. Phys. Chem. Lett.* **2013**, *4*, 779−785.

(19) Kawaguchi, K.; Hirota, E. Infrared Diode-Laser Spectroscopy of FDF. *J. Mol. Struct.* **1995**, *352*, 389−394.

(20) Roscioli, J. R.; Johnson, M. A. Isomer-Specific Spectroscopy of the $(H_2O)_8^-$ Cluster Anion in the Intramolecular Bending Region by Selective Photodepletion of the More Weakly Electron Binding Species (Isomer II). *J. Chem. Phys.* **2007**, *126*, 024307.

(21) Asmis, K. R.; Neumark, D. M.; Bowman, J. M. Gas Phase Vibrational Spectroscopy of Strong Hydrogen Bonds. In *Hydrogen Transfer Reactions*; Hynes, J. T., Klinman, J. P., Limbach, H.-H., Schowen, R. L., Eds.; Wiley-VCH: Weinheim, Germany, 2007; pp 53−78.

(22) Asmis, K. R.; Neumark, D. M. Vibrational Spectroscopy of Microhydrated Conjugate Base Anions. *Acc. Chem. Res.* **2012**, *45*, 43−52.

(23) Zhou, J.; Santambrogio, G.; Brümmer, M.; Moore, D. T.; Meijer, G.; Neumark, D. M.; Asmis, K. R. Infrared Spectroscopy of Hydrated Sulfate Dianions. *J. Chem. Phys.* **2006**, *125*, 111102.

(24) Bush, M. F.; Saykally, R. J.; Williams, E. R. Evidence for Water Rings in the Hexahydrated Sulfate Dianion from IR Spectroscopy. *J. Am. Chem. Soc.* **2007**, *129*, 2220−2221.

(25) Yacovitch, T. I.; Wende, T.; Jiang, L.; Heine, N.; Meijer, G.; Neumark, D. M.; Asmis, K. R. Infrared Spectroscopy of Hydrated Bisulfate Anion Clusters: $HSO_4^-(H_2O)_{(1-16)}$. *J. Phys. Chem. Lett.* **2011**, *2*, 2135−2140.

(26) Lambrecht, D. S.; McCaslin, L.; Xantheas, S. S.; Epifanovsky, E.; Head-Gordon, M. Refined Energetic Ordering for Sulphate−Water (*n* = 3−6) Clusters Using High-Level Electronic Structure Calculations. *Mol. Phys.* **2012**, *110*, 2513−2521.

(27) Wan, Q.; Spanu, L.; Galli, G. Solvation Properties of Microhydrated Sulfate Anion Clusters: Insights from *ab Initio* Calculations. *J. Phys. Chem. B* **2012**, *116*, 9460−9466.

(28) Yacovitch, T. I.; Heine, N.; Brieger, C.; Wende, T.; Hock, C.; Neumark, D. M.; Asmis, K. R. Communication: Vibrational Spectros-

copy of Atmospherically Relevant Acid Cluster Anions: Bisulfate Versus Nitrate Core Structures. *J. Chem. Phys.* **2012**, *136*, 241102.
(29) Yeh, L. I.; Okumura, M.; Myers, J. D.; Price, J. M.; Lee, Y. T. Vibrational Spectroscopy of the Hydrated Hydronium Cluster Ions $H_3O^+\cdot(H_2O)_n$ (n = 1, 2, 3). *J. Chem. Phys.* **1989**, *91*, 7319−7330.
(30) Bailey, C. G.; Kim, J.; Dessent, C. E. H.; Johnson, M. A. Vibrational Predissociation Spectra of $I^-\cdot(H_2O)$: Isotopic Labels and Weakly Bound Complexes with Ar and N_2. *Chem. Phys. Lett.* **1997**, *269*, 122−127.
(31) Beck, J. P.; Lisy, J. M. Infrared Spectroscopy of Hydrated Alkali Metal Cations: Evidence of Multiple Photon Absorption. *J. Chem. Phys.* **2011**, *135*, 044302.
(32) Pankewitz, T.; Lagutschenkov, A.; Niedner-Schatteburg, G.; Xantheas, S. S.; Lee, Y. T. Infrared Spectrum of $NH_4^+(H_2O)$: Evidence for Mode Specific Fragmentation. *J. Chem. Phys.* **2007**, *126*, 074307.
(33) Goebbert, D. J.; Meijer, G.; Asmis, K. R. 10 K Ring Electrode Trap−Tandem Mass Spectrometer for Infrared Spectroscopy of Mass Selected Ions. *AIP Conf. Proc.* **2009**, *1104*, 22−29.
(34) Goebbert, D. J.; Wende, T.; Bergmann, R.; Meijer, G.; Asmis, K. R. Messenger-Tagging Electrosprayed Ions: Vibrational Spectroscopy of Suberate Dianions. *J. Phys. Chem. A* **2009**, *113*, 5874−5880.
(35) Oepts, D.; van der Meer, A. F. G.; van Amersfoort, P. W. The Free-Electron-Laser User Facility FELIX. *Infrared Phys. Technol.* **1995**, *36*, 297−308.
(36) Wende, T.; Dobler, J.; Jiang, L.; Claes, P.; Janssens, E.; Lievens, P.; Meijer, G.; Asmis, K. R.; Sauer, J. Infrared Spectroscopic Characterization of the Oxidative Dehydrogenation of Propane by $V_4O_{10}^+$. *Int. J. Mass Spectrom.* **2010**, *297*, 102−106.
(37) Jiang, L.; Wende, T.; Bergmann, R.; Meijer, G.; Asmis, K. R. Gas-Phase Vibrational Spectroscopy of Microhydrated Magnesium Nitrate Ions $[MgNO_3(H_2O)_{1-4}]^+$. *J. Am. Chem. Soc.* **2010**, *132*, 7398−7404.
(38) Wende, T. Gas Phase Infrared Spectroscopy of Mass-Selected Ionic Clusters: Metal Oxides and Microhydrated Anions. Dissertation, Freie Universität, Berlin, 2012.
(39) Gruene, P.; Lyon, J. T.; Fielicke, A. Vibrational Spectroscopy of Strongly Bound Clusters. In *Handbook of Nanophysics: Clusters and Fullerenes*; Sattler, K., Ed.; CRC Press, Taylor & Francis Group: Boca Raton, FL, 2010; Vol. 2, pp 9-1−9-13.
(40) *Gaussian 09,* revision C.01; Gaussian, Inc.: Wallingford, CT, 2010.
(41) *Macromodel*, version 9.9; Schrödinger, LLC: New York, 2011.
(42) Banks, J. L.; Beard, H. S.; Cao, Y. X.; Cho, A. E.; Damm, W.; Farid, R.; Felts, A. K.; Halgren, T. A.; Mainz, D. T.; Maple, J. R.; et al. Integrated Modeling Program, Applied Chemical Theory (IMPACT). *J. Comput. Chem.* **2005**, *26*, 1752−1780.
(43) Grimme, S. Accurate Description of van der Waals Complexes by Density Functional Theory Including Empirical Corrections. *J. Comput. Chem.* **2004**, *25*, 1463−1473.
(44) Mardirossian, N.; Lambrecht, D. S.; McCaslin, L.; Xantheas, S. S.; Head-Gordon, M. The Performance of Density Functionals for Sulfate−Water Clusters. *J. Chem. Theory Comput.* **2013**, *9*, 1368−1380.
(45) Boys, S. F.; Bernardi, F. Calculation of Small Molecular Interactions by Differences of Separate Total Energies−Some Procedures with Reduced Errors. *Mol. Phys.* **1970**, *19*, 553−566.
(46) Horn, A. B.; Sully, K. J. Atr-IR Spectroscopic Studies of the Formation of Sulfuric Acid and Sulfuric Acid Monohydrate Films. *Phys. Chem. Chem. Phys.* **1999**, *1*, 3801−3806.
(47) Givan, A.; Larsen, L. A.; Loewenschuss, A.; Nielsen, C. J. Matrix Isolation Mid- and Far-Infrared Spectra of Sulfuric Acid and Deuterated Sulfuric Acid Vapors. *J. Mol. Struct.* **1999**, *509*, 35−47.
(48) Walrafen, G. E.; Dodd, D. M. Infra-Red Absorption Spectra of Concentrated Aqueous Solutions of Sulphuric Acid. Part 2. H_2SO_4 and HSO_4^- Vibrational Fundamentals and Estimates of $(F^\circ_{298.15} - H^\circ_0)/T$ and $S^\circ_{298.15}$ for H_2SO_4 Gas. *Trans. Faraday Soc.* **1961**, *57*, 1286−1296.
(49) Giguère, P. A.; Savoie, R. The Normal Vibrational Frequencies and the Thermodynamic Functions of H_2SO_4 and D_2SO_4. *J. Am. Chem. Soc.* **1963**, *85*, 287−289.
(50) Querry, M. R.; Waring, R. C.; Holland, W. E.; Earls, L. M.; Herrman, M. D.; Nijm, W. P.; Hale, G. M. Optical-Constants in Infrared for K_2SO_4, $NH_4H_2PO_4$, and H_2SO_4 in Water. *J. Opt. Soc. Am.* **1974**, *64*, 39−46.
(51) Bagratashvili, V. N.; Letokhov, V. S.; Makarov, A. A.; Ryabov, E. A. *Multiple Photon Infrared Laser Photophysics and Photochemistry*; Harwood Academic Publishers GmbH: Amsterdam, 1985.
(52) Oomens, J.; Sartakov, B. G.; Meijer, G.; von Helden, G. Gas-Phase Infrared Multiple Photon Dissociation Spectroscopy of Mass-Selected Molecular Ions. *Int. J. Mass Spectrom.* **2006**, *254*, 1−19.
(53) Schulz, P. A.; Sudbo, A. S.; Krajnovich, D. J.; Kwok, H. S.; Shen, Y. R.; Lee, Y. T. Multi-Photon Dissociation of Polyatomic-Molecules. *Annu. Rev. Phys. Chem.* **1979**, *30*, 379−409.
(54) Jortner, J. Spiers Memorial Lecture on Dynamics from Isolated Molecules to Biomolecules. *Faraday Discuss.* **1997**, *108*, 1−22.
(55) Headrick, J. M.; Bopp, J. C.; Johnson, M. A. Predissociation Spectroscopy of the Argon-Solvated $H_5O_2^+$ "Zundel" Cation in the 1000−1900 cm^{-1} Region. *J. Chem. Phys.* **2004**, *121*, 11523−11526.
(56) Garand, E.; Wende, T.; Goebbert, D. J.; Bergmann, R.; Meijer, G.; Neumark, D. M.; Asmis, K. R. Infrared Spectroscopy of Hydrated Bicarbonate Anion Clusters: $HCO_3^-(H_2O)_{1-10}$. *J. Am. Chem. Soc.* **2010**, *132*, 849−856.
(57) van Heijnsbergen, D.; von Helden, G.; Sartakov, B.; Meijer, G. IR-Rempi Spectroscopy for Thermometry of C_{60}. *Chem. Phys. Lett.* **2000**, *321*, 508−513.
(58) Miller, Y.; Chaban, G. M.; Gerber, R. B. Ab Initio Vibrational Calculations for H_2SO_4 and $H_2SO_4\cdot H_2O$: Spectroscopy and the Nature of the Anharmonic Couplings. *J. Phys. Chem. A* **2005**, *109*, 6565−6574.
(59) Vendrell, O.; Gatti, F.; Meyer, H. D. Full Dimensional (15 Dimensional) Quantum-Dynamical Simulation of the Protonated Water-Dimer IV: Isotope Effects in the Infrared Spectra of $D(D_2O)_2^+$, $H(D_2O)_2^+$, and $D(H_2O)_2^+$ Isotopologues. *J. Chem. Phys.* **2009**, *131*, 034308.
(60) Li, X. H.; Oomens, J.; Eyler, J. R.; Moore, D. T.; Iyengar, S. S. Isotope Dependent, Temperature Regulated, Energy Repartitioning in a Low-Barrier, Short-Strong Hydrogen Bonded Cluster. *J. Chem. Phys.* **2010**, *132*, 244301.
(61) Dietrick, S. M.; Pacheco, A. B.; Phatak, P.; Stevens, P. S.; Iyengar, S. S. Influence of Water on Anharmonicity, Stability, and Vibrational Energy Distribution of Hydrogen-Bonded Adducts in Atmospheric Reactions: Case Study of the OH Plus Isoprene Reaction Intermediate Using Ab Initio Molecular Dynamics. *J. Phys. Chem. A* **2012**, *116*, 399−414.
(62) Gerber, R. B.; Sebek, J. Dynamics Simulations of Atmospherically Relevant Molecular Reactions. *Int. Rev. Phys. Chem.* **2009**, *28*, 207−222.
(63) Hammer, N. I.; Diken, E. G.; Roscioli, J. R.; Johnson, M. A.; Myshakin, E. M.; Jordan, K. D.; McCoy, A. B.; Huang, X.; Bowman, J. M.; Carter, S. The Vibrational Predissociation Spectra of the $H_5O_2^+\cdot Rg_n$ (Rg = Ar, Ne) Clusters: Correlation of the Solvent Perturbations in the Free OH and Shared Proton Transitions of the Zundel Ion. *J. Chem. Phys.* **2005**, *122*, 244301.
(64) Kamrath, M. Z.; Relph, R. A.; Guasco, T. L.; Leavitt, C. M.; Johnson, M. A. Vibrational Predissociation Spectroscopy of the H_2-Tagged Mono- and Dicarboxylate Anions of Dodecanedioic Acid. *Int. J. Mass Spectrom.* **2011**, *300*, 91−98.